NEUROSCIENCE

Reduction of AMPA receptor activity on mature oligodendrocytes attenuates loss of myelinated axons in autoimmune neuroinflammation

Kirsten S. Evonuk[1], Ryan E. Doyle[1], Carson E. Moseley[2,3], Ian M. Thornell[4]*, Keith Adler[1], Amanda M. Bingaman[1], Mark O. Bevensee[4], Casey T. Weaver[2], Booki Min[5], Tara M. DeSilva[1]†

Glutamate dysregulation occurs in multiple sclerosis (MS), but whether excitotoxic mechanisms in mature oligodendrocytes contribute to demyelination and axonal injury is unexplored. Although current treatments modulate the immune system, long-term disability ensues, highlighting the need for neuroprotection. Glutamate is elevated before T2-visible white matter lesions appear in MS. We previously reported that myelin-reactive T cells provoke microglia to release glutamate from the system x_c^- transporter promoting myelin degradation in experimental autoimmune encephalomyelitis (EAE). Here, we explore the target for glutamate in mature oligodendrocytes. Most glutamate-stimulated calcium influx into oligodendrocyte somas is AMPA receptor (AMPAR)–mediated, and genetic deletion of AMPAR subunit GluA4 decreased intracellular calcium responses. Inducible deletion of GluA4 on mature oligodendrocytes attenuated EAE and loss of myelinated axons was selectively reduced compared to unmyelinated axons. These data link AMPAR signaling in mature oligodendrocytes to the pathophysiology of myelinated axons, demonstrating glutamate regulation as a potential neuroprotective strategy in MS.

INTRODUCTION

Multiple sclerosis (MS) is a neuroinflammatory demyelinating disease of the central nervous system (CNS) that results in progressive disability by causing demise to myelin and axons. Damage to the myelin sheath impairs propagation of nerve impulses. Although myelin can be regenerated by oligodendrocyte progenitor cells (OPCs), this process is fairly inefficient, leaving axons vulnerable to injury and eventual degeneration. Most MS cases are diagnosed as relapsing-remitting, where disease symptoms develop, followed by periods of cessation termed remission. A relapse is defined as a clinical event involving the onset of neurological symptoms; however, the number of inflammatory events in the CNS is far greater than the number of relapses in patients with MS (*1*). This may explain why immunomodulatory drugs used to treat patients with MS initially reduce relapses and improve quality of life; yet, long-term disease progression still proceeds without remedy (*2*). Therefore, therapeutic interventions for CNS protection are necessary for long-term improvement. One such target is glutamate, which is thought to play an important role in the pathophysiology of MS.

Increased concentrations of glutamate in the cerebrospinal fluid (CSF) (*3*), plasma (*4*), and acute lesions (*5*) have been reported in patients with MS. Enhanced levels of glutamate in MS are associated with decreased brain volume (*6*). More recently, elevated levels of glutamate are detected before the appearance of new T2-visible white matter lesions, implicating glutamate as an important excitotoxin in MS (*7*). Consistent with these findings, we previously reported that myelin-reactive T cells provoke microglia to release glutamate from the system x_c^- transporter, promoting myelin degradation in experimental autoimmune encephalomyelitis (EAE) (*8*). Here, we focus on the target for excitotoxic glutamate.

Similar to neurons, oligodendrocytes express ionotropic glutamate receptors that render them vulnerable to excitotoxicity, i.e., the pathological overstimulation of glutamate receptors resulting in calcium-mediated cell death. Excitotoxicity has been linked to MS by amelioration of EAE using AMPA-type glutamate receptor (AMPAR) antagonists administered by intraperitoneal injection (*9*, *10*) and by global genetic deletion of the GluA3 AMPAR subunit (*11*). However, AMPAR expression on T cells regulates their activation (*12*) and chemotactic migration (*13*), which could modulate their effector function and their extravasation into the CNS. Furthermore, neurons express AMPARs, making it unclear whether damage to myelin is facilitated subsequent to neuronal dysfunction. Therefore, direct evidence of excitotoxicity specific to oligodendrocytes in EAE has not been demonstrated.

Excitotoxicity to oligodendrocytes is regulated through GluA2-free calcium-permeable AMPARs with a combination of subunits GluA1, GluA3, and GluA4 (*14*). Here, we show that GluA4 is robustly expressed on mature oligodendrocytes in the adult rodent consistent with their expression in the adult human white matter (*15*). We also found that most of the glutamate-stimulated calcium influx in oligodendrocyte cell bodies is AMPAR-mediated and Cre recombinase-mediated deletion of the GluA4 AMPAR subunit decreased calcium responses. Selective deletion of GluA4 on mature oligodendrocytes using inducible PLPcreER ameliorated clinical symptoms in the chronic phase of EAE. Consistent with diminished clinical severity, AMPAR-deficient mice had less myelin damage, a reduction in axonal loss, and a decrease in the production of amyloid precursor protein (APP) (a marker of axonal injury) in spinal cord white matter. To determine whether targeted deletion of AMPARs on mature oligodendrocytes specifically affected myelinated axons as opposed to unmyelinated axons in EAE, axonal integrity was evaluated at the ultrastructural level by electron microscopy. There was a statistically significant reduction in myelinated axons but not unmyelinated axons, suggesting that deletion of AMPARs on mature oligodendrocytes

[1]Department of Neurosciences, Lerner Research Institute, Cleveland Clinic Foundation, Cleveland, OH, USA. [2]Department of Pathology, University of Alabama at Birmingham, Birmingham, AL, USA. [3]University of California, San Francisco, CA, USA. [4]Department of Cell, Developmental and Integrative Biology, University of Alabama at Birmingham, Birmingham, AL, USA. [5]Department of Immunology, Lerner Research Institute, Cleveland Clinic Foundation, Cleveland, OH, USA.
*Present address: University of Iowa, Iowa, IA, USA.
†Corresponding author. Email: desilvt@ccf.org

is selectively protective to axons with myelin. These data provide evidence that selectively deleting the AMPAR subunit GluA4 in mature oligodendrocytes not only reduces demyelination but also protects myelinated axons from injury in EAE. Thus, therapeutic strategies to regulate glutamate homeostasis have important clinical ramifications for protecting the CNS.

RESULTS

Inducible deletion of GluA4 impairs glutamate-induced AMPAR-mediated calcium signaling in the oligodendrocyte soma

We previously reported that microglia stimulated with interferon-γ and tumor necrosis factor–α (TNF-α) caused death of mature oligodendrocytes that could be attenuated by inhibiting an excitotoxic source of glutamate or blocking AMPARs with 2,3-Dioxo-6-nitro-1,2,3,4-tetrahydrobenzo[*f*]quinoxaline-7-sulfonamide (NBQX) but not *N*-methyl-D-aspartate (NMDA)–type glutamate receptors (NMDARs) with MK-801 (*8*). Consistent with these data, primary cultured mature oligodendrocytes loaded with the calcium-sensitive dye Fura-2 acetoxymethyl ester (AM) responded to glutamate stimulation, with an increase in intracellular calcium (Ca_i^{2+}) in the cell soma that was nearly completely inhibited by the AMPAR antagonist NBQX (93% inhibition, SEM ± 2%; fig. S1, A and D). We observed a similar inhibition with NBQX after stimulation with the AMPA agonist (97% inhibition, SEM ± 1%; fig. S1, B and D). The glutamate response elicited in primary mature oligodendrocytes was partially inhibited by the noncompetitive NMDAR antagonist MK-801 (40% inhibition, SEM ± 7%; fig. S1, C and D). On the basis of these experimental results and a lack of efficacy in NMDAR deletion in reducing EAE symptoms (*16*), we used PLPcreER mice in which tamoxifen-inducible cre expression is driven under control of the oligodendrocyte-specific PLP promoter (*17*) to delete the AMPAR subunit GluA4 specifically from mature oligodendrocytes in adult mice. The $GluA4^{fl/fl}$ mouse line was previously characterized using a neuron-specific cre, which significantly reduced AMPAR currents (*18*). Oligodendrocytes express GluA4 throughout development (*19*, *20*), and GluA4 is abundant in adult human white matter (*15*), rodent spinal cord white matter (*21*), and rodent optic nerve oligodendrocytes (*22*). These data indicate that GluA4 deletion in mature oligodendrocytes will decrease AMPAR-mediated Ca^{2+} influx. Therefore, we tested the hypothesis that targeted deletion of GluA4 in oligodendrocytes reduces AMPAR-mediated calcium influx. In the spinal cord white matter of adult $PLPcreER^{+}$;$GluA4^{fl/fl}$ mice, GluA4 expression (2 weeks after tamoxifen induction) was substantially reduced in mature oligodendrocyte somas compared to $PLPcreER^{-}$;$GluA4^{fl/fl}$ mice (Fig. 1A and quantification in fig. S2A) but remained unchanged in glial fibrillary acidic protein (GFAP) immunoreactive astrocytes (Fig. 1B and quantification in fig. S2B) and a subset of motor neurons (Fig. 1C and quantification in fig. S2C). Furthermore, quantification of GluA4 in ionized calcium binding adaptor molecule 1 (Iba1) immunoreactive myeloid cells (fig. S2, D and F) and any cellular structure negative for adenomatous polyposis coli clone CC1 (CC1) (fig. S2E) was also not statistically different. Expression of GluA1-3 in oligodendrocytes remained unchanged (quantified in fig. S2A and images in fig. S3). Transcript expression of GluA1-4 reflected the results found at the protein level with a statistically significant reduction in Gria4 but not Gria1-3 (fig. S4A). As reduced AMPAR signaling due to deletion of GluA4 could result in compensatory expression of other ionotropic glutamate receptor subunits, we next explored whether a reduction of GluA4 affected the expression of kainate and NMDARs (fig. S4, B and C). No compensatory up-regulation was observed; however, Grik3, encoding the GluK3 (GluR7) kainate receptor subunit, was significantly reduced in $PLPcreER^{+}$;$GluA4^{fl/fl}$ compared to $PLPcreER^{-}$;$GluA4^{fl/fl}$ white matter. Expression of NMDAR subunit transcript was unchanged (fig. S4C).

To demonstrate AMPA/kainite receptor–mediated Ca_i^{2+} responses in oligodendrocytes ex vivo, we preincubated optic nerves from $PLPcreER^{+}$;$GluA4^{+/+}$;$tdTomato^{+}$ and $PLPcreER^{+}$;$GluA4^{fl/fl}$;$tdTomato^{+}$ mice with Oregon Green 488 BAPTA-1 (OGB-1), a fluorescent calcium indicator. After stimulation with glutamate, fluorescent $TdTomato^{+}$ oligodendrocytes exhibited an increase in Ca_i^{2+} in the cell soma (Fig. 2, A and B) that was largely inhibited by the AMPA/kainite receptor antagonist NBQX (Fig. 2, B to D). Ex vivo optic nerves from $PLPcreER^{+}$;$GluA4^{fl/fl}$;$tdTomato^{+}$ mice showed a statistically significant reduction in maximum and overall Ca_i^{2+} in the cell soma compared to $PLPcreER^{+}$;$GluA4^{+/+}$;$tdTomato^{+}$ in response to glutamate that was principally blocked by NBQX (Fig. 2, B to D). These data provide evidence that selective deletion of GluA4 in oligodendrocytes confers a functional impairment in AMPA/kainite receptor–mediated intracellular calcium in the cell soma in response to glutamate.

Inducible deletion of GluA4 from mature oligodendrocytes in adult mice using PLPcreER ameliorates clinical scores and reduces myelin degradation in EAE

Constitutive deletion of AMPARs during development results in a reduction in myelin thickness (*23*). To avoid confounding developmental defects in myelination, adult mice were tamoxifen-induced to selectively delete GluA4 in mature oligodendrocytes. To further confirm that inducible deletion of GluA4 in mature myelin does not affect myelin/axonal integrity in naïve mice, we performed electron microscopy of spinal cord white matter from 9-week-old $PLPcreER^{+}$:$GluA4^{fl/fl}$ [knockout (KO)] and $PLPcreER^{-}$:$GluA4^{fl/fl}$ littermate control [wild-type (WT)] mice 3 weeks after tamoxifen induction. The g-ratio (ratio of axon diameter to axon and myelin diameter) measurements (fig. S5, A to C) and cumulative frequency distribution of g-ratios (fig. S6A) revealed no statistical difference between WT and KO, providing evidence that myelin thickness in the lumbar ventral white matter of the spinal cord was unaltered in KO mice. In addition, lumbar ventral white matter axons in KO mice had normal percentage of myelinated (fig. S5D) and unmyelinated (fig. S5E) axons, and total number of axons was unchanged (fig. S5F). Axon diameter was also normal as indicated by no shift in cumulative frequency distribution of myelinated (fig. S6B) or unmyelinated (fig. S6C) axons. Together, these results suggest that myelin and axons are unaltered in naïve animals after inducible deletion of GluA4 from mature oligodendrocytes. To determine whether AMPARs mediate excitotoxic damage to myelin during autoimmune neuroinflammation, we subjected adult 9-week-old $PLPcreER^{+}$:$GluA4^{fl/fl}$ (KO) and $PLPcreER^{-}$:$GluA4^{fl/fl}$ littermate control (WT) mice to EAE 2 weeks after tamoxifen induction to activate recombination. EAE was significantly less severe in mice deficient in AMPAR function selectively on mature oligodendrocytes (KO) compared to control (WT) (Fig. 3A). To confirm that the specificity of PLPcreER for oligodendrocytes was not affected after EAE, we stained spinal cords from $PLPcreER^{+}$;$GluA4^{fl/fl}$;$tdTomato^{+}$ mice with anti-neuronal nuclei (NeuN), anti-GFAP, and anti-Iba1. TdTomato did not colocalize

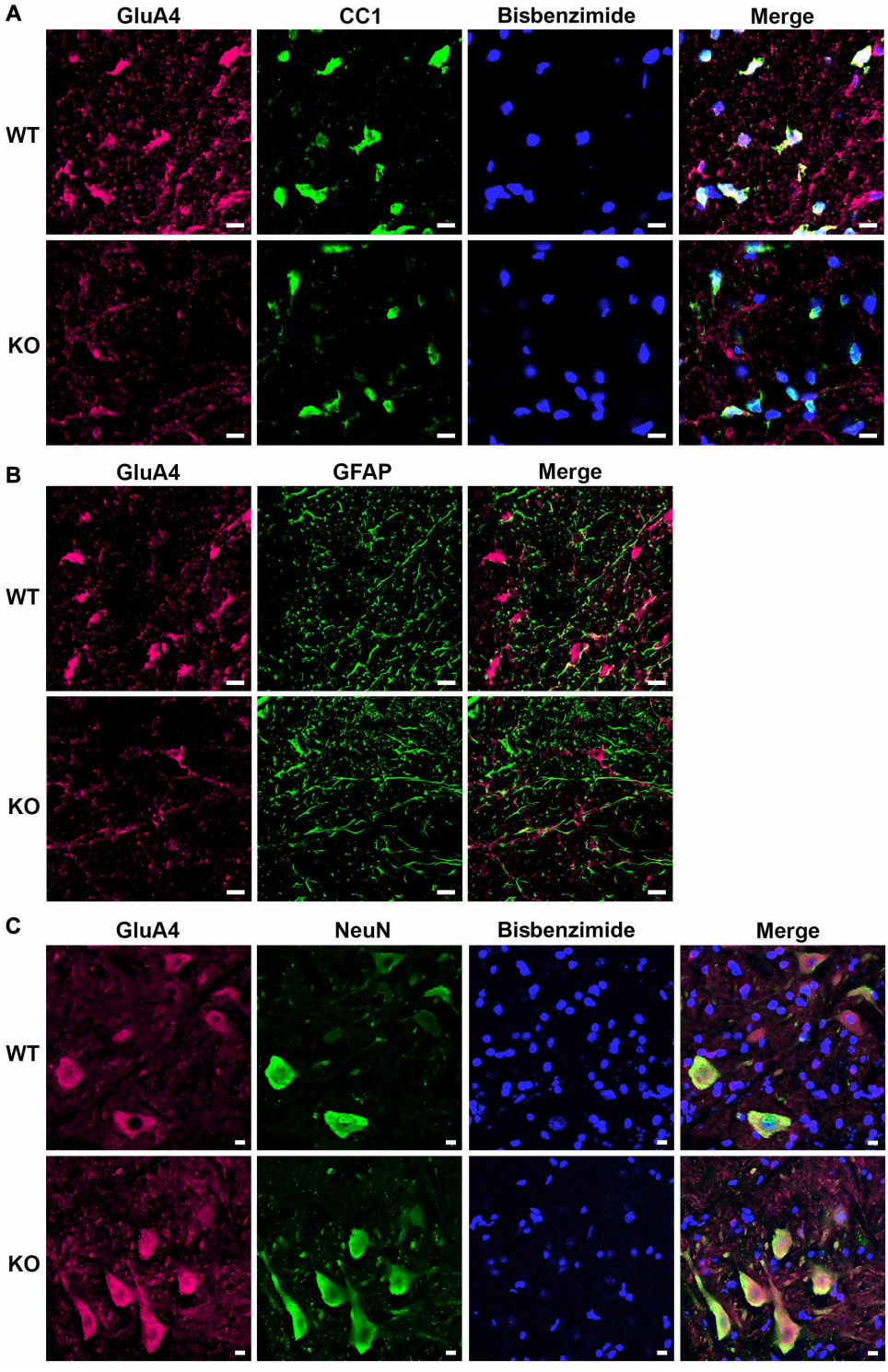

Fig. 1. The GluA4 AMPAR subunit is reduced in adult spinal cord oligodendrocytes from PLPcreER^{+};GluA4$^{fl/fl}$ compared to PLPcreER^{-};GluA4$^{fl/fl}$ mice. Mice were tamoxifen-induced at 6 weeks of age and euthanized for immunofluorescence staining at 8 weeks of age. Representative confocal images of PLPcreER^{-};GluA4$^{fl/fl}$ (WT) versus PLPcreER^{+};GluA4$^{fl/fl}$ (KO) mouse lumbar spinal cords. (**A**) Images taken in lateral funiculus white matter. Far-red (pseudocolored magenta) immunofluorescence represents anti-GluA4 (first column). Green immunofluorescence represents the mature oligodendrocyte marker anti-CC1 (second column). Blue fluorescence represents the nuclear marker bisbenzimide (third column). All images are merged in the final column (Merge). (**B**) Images taken in lateral funiculus white matter. Far-red (pseudocolored magenta) immunofluorescence represents anti-GluA4 (first column). Green immunofluorescence represents the astrocyte marker anti-GFAP (second column). All images are merged in the final column (Merge). (**C**) Images taken in ventral gray matter. Far-red (pseudocolored magenta) immunofluorescence represents anti-GluA4 (first column). Green immunofluorescence represents the neuronal marker NeuN (second column). Blue fluorescence represents the nuclear marker bisbenzimide (third column). All images are merged in the final column (Merge). Images are representative of $n = 4$ mice per genotype. Scale bars, 10 μm.

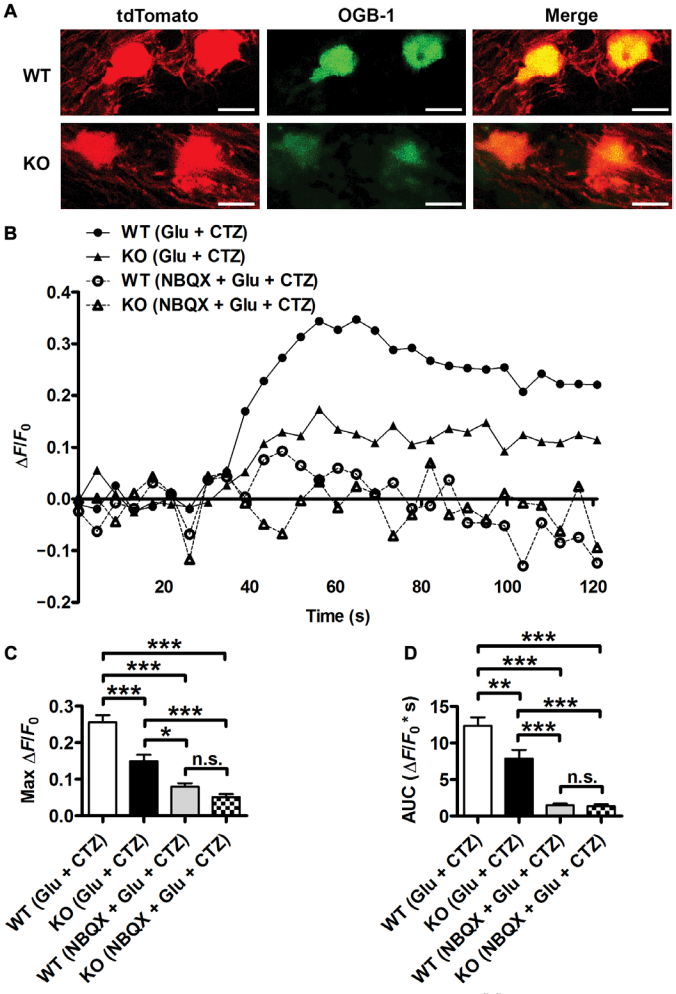

Fig. 2. AMPARs on oligodendrocytes in PLPcreER$^+$;GluA4$^{fl/fl}$;tdTomato$^+$ mice are functionally impaired. (**A**) Representative images of tdTomato$^+$ oligodendrocytes in PLPcreER$^+$;GluA4$^{+/+}$;tdTomato$^+$ (WT) and PLPcreER$^+$;GluA4$^{fl/fl}$;tdTomato$^+$ (KO) mouse optic nerves (left column) loaded with calcium indicator OGB-1 (middle column), and merged image (right column) during peak response to stimulation with glutamate and cyclothiazide (CTZ). Scale bars, 10 μm. (**B**) Representative traces of $\Delta F/F_0$ for 120 s representing relative Ca_i^{2+} concentration in tdTomato$^+$ oligodendrocytes from PLPcreER$^+$;GluA4$^{+/+}$;tdTomato$^+$ (WT; black circles) and PLPcreER$^+$;GluA4$^{fl/fl}$;tdTomato$^+$ (KO; black triangles) mice treated with Glu + CTZ (solid lines), or WT (open circles) and KO (open triangles) mice treated with NBQX + Glu + CTZ (dashed lines). (**C**) Maximum $\Delta F/F_0$ of Ca_i^{2+} responses during treatment with Glu + CTZ or NBQX + Glu + CTZ. (**D**) Area under the curve (AUC) of $\Delta F/F_0$ over the first 120 s of treatment with Glu + CTZ or NBQX + Glu + CTZ. For (C) and (D), statistical differences were determined using one-way analysis of variance (ANOVA) ($P < 0.0001$ for each test) with Bonferroni's multiple comparison test. *$P < 0.05$, **$P < 0.01$, ***$P < 0.001$. n.s., not significant. For (C) and (D), quantification includes $n = 94$ WT (Glu + CTZ) cells from three nerves, $n = 88$ KO (Glu + CTZ) cells from three nerves, $n = 50$ WT (NBQX + Glu + CTZ) cells from three nerves, and $n = 86$ KO (NBQX + Glu + CTZ) cells from two nerves. Mice were euthanized at P9.

with neurons (NeuN), astrocytes (GFAP), or microglia (Iba1) (fig. S7). Furthermore, expression of AMPARs after EAE induction (fig. S8) was consistent with the expression found before induction of EAE (Fig. 1 and fig. S3). To evaluate whether KO mice had a reduction in myelin damage compared to WT in the chronic phase of EAE (35 days after EAE induction), we quantified anti–myelin basic protein (MBP) 3,3′-diaminobenzidine (DAB) staining of spinal cord myelin. We observed a significantly higher optical density (OD) of myelin staining in total lumbar spinal cord white matter of AMPAR-deficient mice compared to control (Fig. 3, B to E), indicating that AMPARs mediate excitotoxic damage to myelin in autoimmune neuroinflammation. To determine whether a reduction in myelin damage influenced reactive gliosis, we assessed DAB staining for astrocytes (anti-GFAP) and the myeloid lineage (anti-Iba1) in whole spinal cord sections. Percent area for astrocyte staining was not significantly reduced in KO mice compared to control (Fig. 3, F to I), while anti-Iba1 staining was statistically decreased in the lumbar region (Fig. 3, J to M). Previous studies have shown that markers of the myeloid lineage correlate with removal of myelin debris (*24*). Together, these data suggest that a functional reduction in AMPAR-mediated intracellular calcium responses reduced excitotoxic damage to myelin.

Inducible deletion of GluA4 from mature oligodendrocytes in EAE reduces axonal damage

Inducible deletion of GluA4 selectively in mature oligodendrocytes attenuated clinical scores consistent with myelin preservation in adult mice subjected to EAE. To investigate whether blocking AMPAR-mediated excitotoxicity to myelin affects axon integrity, we used three-dimensional (3D) reconstruction of axons in PLPcreER$^-$;GluA4$^{fl/fl}$ (WT) and PLPcreER$^+$;GluA4$^{fl/fl}$ (KO) mice 35 days after EAE induction. In the lumbar ventral white matter, where demyelination is prominent during EAE, loss of SMI-312–immunopositive axons was apparent in WT compared to KO mice in the chronic phase of EAE (day 35 after EAE induction; Fig. 4). We also observed irregularities in axonal organization and size in WT compared to KO mice (Fig. 4, A to C, and movies S1 and S2). Swollen axons indicative of the presence of axonal ovoids (Fig. 4, B and C) as described in postmortem MS brains (*25*) were prevalent in WT compared to KO mice. KO mice exhibited a statistically significant preservation of axon number (Fig. 4D). To further explore axonal damage, we performed immunostaining of anti-APP (APP A4) staining in the lumbar spinal cord white matter (Fig. 5A). APP accumulation in axons results from axonal damage (*26*), and we observed APP$^+$ puncta colocalized with axons (Fig. 5, C to E). Furthermore, we found a reduced number of APP$^+$ puncta in the dorsal column white matter of KO mice compared to WT mice (Fig. 5B). However, in the ventral white matter where there is a substantial loss of axons (Fig. 4), no difference in the number of APP$^+$ puncta was detected. These data are consistent with other studies demonstrating the transient nature of APP expression in MS and EAE lesions, with greater accumulation in acute lesions than in chronic lesions, suggesting that when there is loss of axons, there is loss of APP$^+$ puncta (*27*).

To test the hypothesis that selectively deleting AMPAR function on mature oligodendrocytes confers protection to myelinated axons as opposed to unmyelinated axons in EAE, we performed assessments at the ultrastructural level. We first assessed the lumbar ventral white matter, where demyelination is prominent during EAE, with toluidine blue, which only stains myelinated axons. KO EAE mice had preserved numbers of myelinated axons compared to WT EAE mice (Fig. 6, A and B). We used electron microscopy to assess the total number of axons, including myelinated as opposed to unmyelinated axons. Consistent with observations by confocal 3D reconstruction (Fig. 4), the total number of axons was higher in KO compared to WT EAE mice (Fig. 6C). Furthermore, consistent with

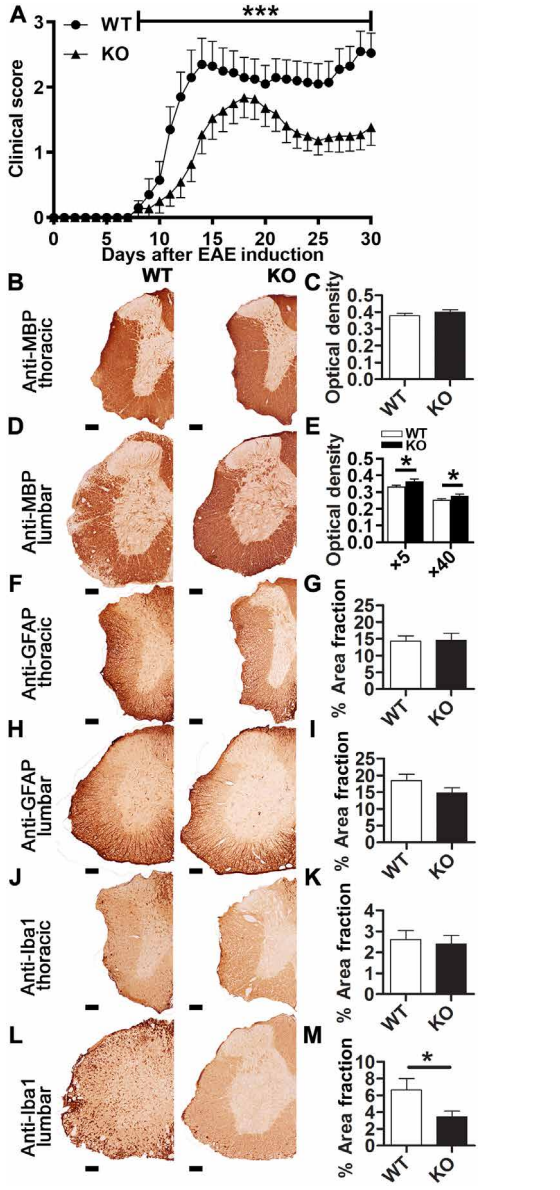

Fig. 3. Inducible reduction of AMPAR signaling in mature myelinating oligodendrocytes attenuates EAE consistent with reduced demyelination. (**A**) EAE clinical scores (means ± SEM) of PLPcreER^{-};GluA4$^{fl/fl}$ littermate controls (WT; circles; $n = 20$) and PLPcreER^{+};GluA4$^{fl/fl}$ (KO; triangles; $n = 22$) mice. Statistical differences were determined from disease onset (days 8 to 30 after EAE induction; bar above graph) using a two-tailed Mann-Whitney test, $^{***}P < 0.0001$. MBP staining of the thoracic (**B**) and lumbar (**D**) spinal cords. Quantification of OD of the thoracic (**C**) and lumbar (**E**) spinal cords. Statistical differences were determined using a two-tailed unpaired *t* test ($P = 0.3188$ for thoracic at ×5 magnification, $^{*}P = 0.0288$ for lumbar at ×5 magnification, and $^{*}P = 0.0280$ for lumbar at ×40 magnification). GFAP staining of thoracic (**F**) and lumbar (**H**) spinal cords. Quantification of percent area stained of the thoracic (**G**) and lumbar (**I**) spinal cords at ×5 magnification. Statistical differences were determined using a two-tailed unpaired *t* test ($P = 0.9308$ for thoracic and $P = 0.1347$ for lumbar). Iba1 staining of the thoracic (**J**) and lumbar (**L**) spinal cords. Quantification of percent area stained of the thoracic (**K**) and lumbar (**M**) spinal cords at ×5 magnification. Statistical differences were determined using a two-tailed unpaired *t* test ($P = 0.7297$ for thoracic and $^{*}P = 0.0275$ for lumbar). Scale bars, 100 μm. All data are expressed as means ± SEM, including $n = 5$ to 6 WT and 7 to 8 KO mice induced with EAE and euthanized on day 35 after EAE induction, 1 to 4 spinal cords sections per mouse.

toluidine blue staining, KO had higher numbers of myelinated axons compared to WT EAE mice quantified using electron microscopy (Fig. 6, D and E). In addition, the percentage of myelinated axons was the same between KO EAE and naïve mice (Fig. 6F) but not WT EAE mice, demonstrating a preservation of myelinated axons in KO EAE mice. Unmyelinated axon numbers, however, did not differ between WT and KO EAE groups (Fig. 6, G and H), suggesting that targeted deletion of GluA4 in mature oligodendrocytes confers selective protection to myelinated axons. Conversely to the percentage of myelinated axons, the percentage of unmyelinated axons was higher in the WT EAE mice than in the naïve and KO EAE mice (Fig. 6I), demonstrating that there is less demyelination in the KO EAE group compared to WT EAE.

DISCUSSION

This study demonstrates that a functional reduction in AMPAR activity on mature oligodendrocytes ameliorates clinical presentation, reduces myelin damage, and specifically attenuates loss of myelinated axons in EAE. Selective deletion of the GluA4 AMPAR subunit on oligodendrocytes reduced calcium responses in the cell soma but did not affect myelin or axonal integrity in naïve mice. Therefore, these data support that the AMPAR is a conduit for glutamate-induced calcium influx into mature oligodendrocytes to facilitate excitotoxic damage to myelin and a concomitant loss of axons in a model of autoimmune inflammatory demyelination. Furthermore, our data show that selectively reducing AMPAR signaling in myelin promotes axonal integrity, particularly providing protection to myelinated axons as demonstrated by ultrastructural analysis and providing evidence, at least in part, that damage to axons is secondary to myelin damage in EAE.

Although glutamate is essential for excitatory synaptic transmission, overstimulation of ionotropic glutamate receptors is a pathological process initiating excessive calcium influx that results in excitotoxicity to neurons. This is an important mechanism involved in neurodegenerative diseases. Oligodendrocytes also express ionotropic glutamate receptors and are vulnerable to excitotoxicity (*14*). In animal models of perinatal hypoxic-ischemic injury, damage to developing oligodendrocytes was blocked by AMPAR and NMDAR antagonists (*28*, *29*). Although immunofluorescence studies in the rodent and human brain have shown that GluR2-lacking AMPARs (which confer calcium permeability) are more highly expressed on developing oligodendrocytes (*19*, *20*), mature myelinating oligodendrocytes in the adult brain are vulnerable to AMPAR-mediated excitotoxic damage induced by chemical ischemia and AMPAR agonists (*22*, *30*, *31*). During chemical ischemia in adult white matter, AMPARs mediate excitotoxic damage to the cell body, whereas NMDARs mediate excitotoxic damage to the myelin sheath (*30*), providing a specific regional organization after maturation. Our ex vivo calcium imaging data demonstrate that genetic deletion of the GluA4 AMPAR subunit decreased calcium responses in the oligodendrocyte cell body. This is not only consistent with a statistically significant decrease in GluA4 protein expression but may also be partially attributed to the reduction in the low-affinity kainite receptor 3 (Grik3). Glutamate-stimulated calcium influx was nearly completely blocked by NBQX, an AMPA/kainite receptor antagonist, indicating an AMPA/kainite receptor–mediated response. In primary mature oligodendrocytes cultured from rodent forebrain, we also show that glutamate-stimulated calcium influx into the soma was

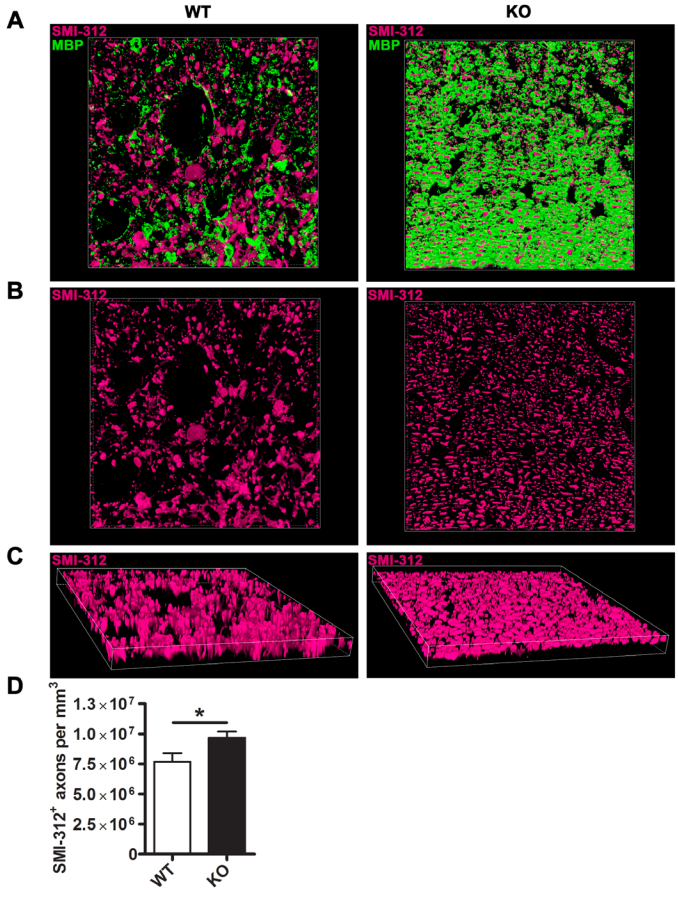

Fig. 4. Inducible reduction of AMPAR signaling in mature oligodendrocytes attenuates axonal loss in EAE. (**A** to **C**) Alpha-blended 3D representations of confocal *z*-stacks (112.71 μm by 112.71 μm by 9.00 μm) of spinal cord ventral funiculus from PLPcreER^{-};GluA4$^{fl/fl}$ (WT; first column) and PLPcreER^{+};GluA4$^{fl/fl}$ (KO; second column) mice. Far-red (pseudocolored magenta) immunofluorescence represents anti–SMI-312 (neurofilament), and green immunofluorescence represents anti-MBP. Top-down view in (A) and (B) and angled view in (C). (**D**) Quantification of SMI-312^{+} axons per cubic millimeter (means ± SEM), $n = 6$ WT and 8 KO mice, 3 to 4 3D *z*-stacks from two sections per mouse euthanized 35 days after EAE induction. Statistical differences were determined using a two-tailed unpaired *t* test, $^{*}P = 0.0248$.

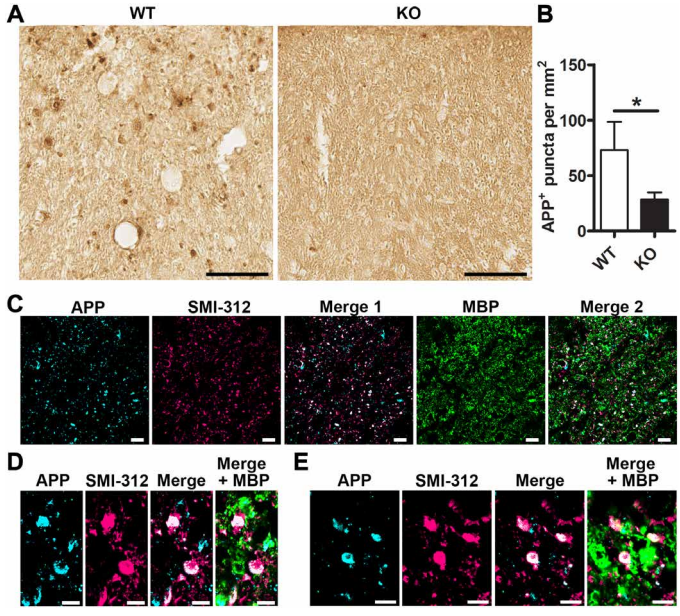

Fig. 5. Inducible reduction of AMPAR signaling in oligodendrocytes attenuates axonal damage in EAE. (**A**) Anti–APP A4 staining of lumbar dorsal white matter. Scale bars, 50 μm. (**B**) Quantification of anti–APP A4^{+} puncta in dorsal white matter of lumbar spinal cords (means ± SEM), $n = 6$ PLPcreER^{-};GluA4$^{fl/fl}$ (WT) and 8 PLPcreER^{+};GluA4$^{fl/fl}$ (KO) mice, 2 to 4 sections per mouse, euthanized 33 days after EAE induction. Statistical differences were determined using a two-tailed unpaired *t* test, $^{*}P = 0.0412$. (**C**) Colocalization of anti–APP A4 with anti–SMI-312 (neurofilament) in WT mouse spinal cord white matter. Red (pseudocolored cyan) immunofluorescence represents anti–APP A4 (first column). Far-red (pseudocolored magenta) immunofluorescence represents anti–SMI-312 (second column). Anti–APP A4 and anti–SMI-312 are merged in the third column (Merge 1). Green immunofluorescence represents anti-MBP (fourth row). All images are merged in the final column (Merge 2). Images are representative of $n = 3$ WT mice. Scale bars, 10 μm. (**D** and **E**) Magnified images of APP^{+}/SMI-312^{+} axons in the spinal cord white matter of WT mice. Scale bars, 5 μm.

also nearly completely blocked with NBQX. Protein expression and calcium influx are not completely abolished in AMPA/kainite receptor–deficient oligodendrocytes, which may serve important signaling roles necessary for normal physiology (*23*).

While most of the glutamate-stimulated calcium influx in the oligodendrocyte soma appeared to be AMPA/kainite receptor–mediated, approximately 40% of the calcium influx was blocked by the NMDAR antagonist MK-801. Previous studies have also reported NMDAR responses in the mature soma of oligodendrocytes (*32*). Together, these data suggest that in the oligodendrocyte soma, the AMPA/kainite receptor may be the gateway for activation of the NMDAR. This is similar to observations in neurons, where AMPAR activation is necessary to depolarize the cell membrane and relieve the magnesium block to facilitate NMDAR-mediated calcium influx. However, deletion of the obligatory NR1 NMDAR subunit selectively on oligodendrocytes did not attenuate EAE (*16*). In light of the current study, there may be several explanations for this. Overactivation of NMDARs is highly excitotoxic to neurons, which are composed of the conventional heteromeric subunits NR1 and NR2A-D. On the contrary, oligodendrocytes express a unique NMDAR subunit composition. NMDARs on oligodendrocytes contain the NR3 subunit that confers a reduction in calcium permeability (*32*). Oligodendrocytes also express NR1/NR3 excitatory glycine receptors that are not activated by glutamate (*33*). In addition, if the predominant expression of NMDARs resides in the mature myelin sheath, perhaps the small volume of the mature process restricts calcium influx and its effect on mature oligodendrocytes as a whole. Each oligodendrocyte's mature myelinating processes can ensheath multiple axons, making damage to the oligodendrocyte soma amplificatory.

Factors that contribute to the excitotoxic vulnerability of AMPARs must be considered in EAE and MS. The system x_c^- transporter imports cystine for the biosynthesis of glutathione in exchange for export of glutamate (*34*). We previously demonstrated that an important link between inflammation and glutamate dysregulation in autoimmune inflammatory demyelination is the system x_c^- transporter, which is highly up-regulated on microglia as a consequence of T cell activation and promotes myelin degradation (*8*). In addition, we showed that CNS-infiltrating macrophages highly express system x_c^-, making its contribution to the excitotoxic pool of glutamate highly relevant in EAE. Similarly, activated monocytes from patients with MS also

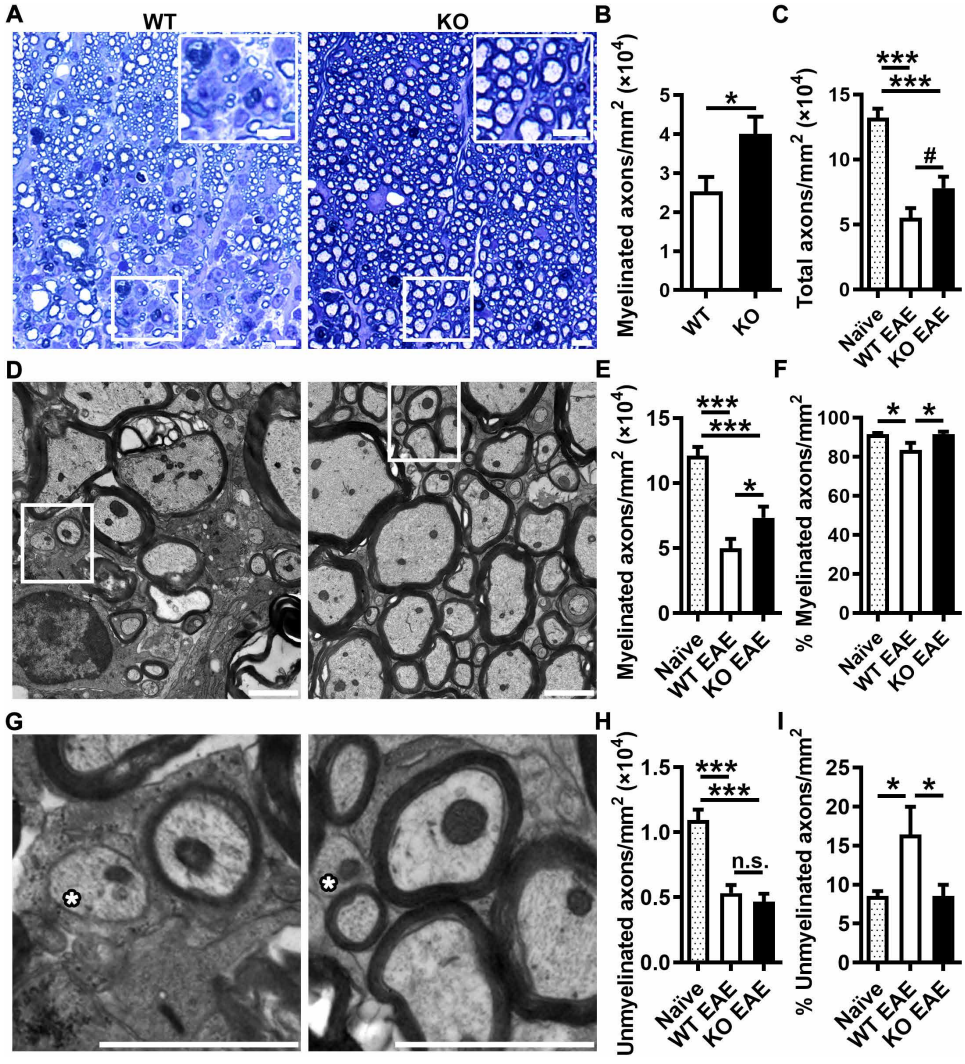

Fig. 6. Inducible reduction of AMPAR signaling in oligodendrocytes reduces loss of myelinated axons in EAE. (**A**) Representative images of ventral funiculus in semithin lumbar spinal cord sections from PLPcreER^{-};GluA4$^{fl/fl}$ (WT) and PLPcreER^{+};GluA4$^{fl/fl}$ (KO) mice stained with toluidine blue. White boxes outline inset areas. Scale bars, 10 μm. (**B**) Quantification of myelinated axons in toluidine blue–stained ventral funiculus of lumbar spinal cords from WT and KO mice, *P = 0.0175. (**C**) Quantification of total number of axons in transmission electron micrograph images of the ventral funiculus of lumbar spinal cords from naïve, WT EAE, and KO EAE mice. Naïve compared to WT EAE, ***P < 0.0001; naïve compared to KO EAE, ***P < 0.0001; WT EAE compared to KO EAE, #P = 0.0565. (**D**) Representative transmission electron micrograph images of ventral funiculus in ultrathin lumbar spinal cord sections from WT and KO mice. Scale bars, 2 μm. (**E**) Quantification of number of myelinated axons over total axons per square millimeter. Naïve compared to WT EAE, ***P < 0.0001; naïve compared to KO EAE, ***P < 0.0001; WT EAE compared to KO EAE, *P = 0.0431. (**F**) Quantification of percentage of myelinated axons over total axons in naïve, WT EAE, and KO EAE mice. Naïve compared to WT EAE, *P = 0.0144; naïve compared to KO EAE, P = 0.9930; WT EAE compared to KO EAE, *P = 0.0144. (**G**) Representative transmission electron micrograph images of ventral funiculus in ultrathin lumbar spinal cord sections from WT and KO mice. Asterisks denote unmyelinated axons. Scale bars, 2 μm. (**H**) Quantification of number of unmyelinated axons over total axons per square millimeter. Naïve compared to WT EAE, ***P < 0.0001; naïve compared to KO EAE, ***P < 0.0001; WT EAE compared to KO EAE, P = 0.5386. (**I**) Quantification of percentage of unmyelinated axons over total axons in naïve, WT EAE, and KO EAE mice. Naïve compared to WT EAE, *P = 0.0144; naïve compared to KO EAE, P = 0.9930; WT EAE compared to KO EAE, *P = 0.0144. All quantifications are expressed as means ± SEM and were performed on n = 6 naïve, 4 WT EAE, and 5 KO EAE mice, six fields per mouse, euthanized 30 days after EAE induction. Statistical differences were determined using a two-tailed unpaired t test (B) or one-way ANOVA with Holm-Sidak's multiple comparison test (C, E, F, H, and I).

up-regulate and release glutamate through the system x_c^- transporter (*35*). Moreover, we previously showed that pharmacological inhibition of system x_c^- after disease onset and immune cell infiltration reduces symptoms of EAE and results in increased myelin integrity (*8*), demonstrating that targeting a source of excitotoxic glutamate is neuroprotective. Correspondingly, elevated levels of glutamate are detected before the appearance of new T2-visible white matter lesions, implicating glutamate as an important excitotoxin to the development of lesions in patients with MS (*7*).

Several studies present compelling evidence that the major regulators of extracellular glutamate are down-regulated in MS and animal models of MS. Excitatory amino acid transporters (EAATs) are extremely efficient in maintaining glutamate homeostasis; however, genetic perturbations in glutamate transporter expression are known to promote excitotoxicity (*36*). Proinflammatory cytokines, particularly TNF-α implicated in the pathology of MS and EAE (*37*, *38*), reduced glutamate transporter expression and function (*39*, *40*). In rodents subjected to EAE, protein expression of glutamate

transporters was reduced (*41*, *42*). In white matter from patients with MS, expression of EAAT1 and EAAT2 was diminished in the perimeter of early and chronic active lesions (*43*). These data support the hypothesis that excess extracellular glutamate cannot be properly regulated by glutamate transporters.

Published data also provide evidence that inflammation enhances excitotoxicity. The cytokine TNF-α enhanced excitotoxic death of oligodendrocytes (*44*). Exposure to TNF-α also increased the surface expression of calcium permeable AMPARs in cultured hippocampal neurons (*45*). A similar phenomenon was reported in MS lesions, where GluA1 was found to be up-regulated in oligodendrocytes, while the expression of GluA2, which reduces calcium permeability when present, remained unchanged (*46*). This suggests that in inflammatory states, oligodendrocytes may be more susceptible to the effects of excitotoxicity than during normal physiological conditions. While infiltrating immune cells has been documented in MS brains and animal models of EAE providing a strong link between inflammation and glutamate dysregulation in cerebral white matter, diffuse reactive gliosis has also been documented in gray matter regions in MS (*47*). This suggests that while infiltrating immune cells produces an acute excitotoxic lesion in white matter, there may be a more subtle imbalance in glutamate homeostasis that contributes to the long-term gray matter atrophy observed in patients with MS.

Newly proliferated OPCs that appear in lesions from human MS postmortem brains and animal model of MS may also be vulnerable to excitotoxic mechanisms or hyperactivation of glutamate receptors. This may cause death of OPCs, reducing the number available for remyelination, or lock OPCs in an undifferentiated state. A significant reduction in the number of OPCs was observed in chronic active lesions from MS brains, attributed to a change in migration and/or death (*48*). Another study illustrated differentiated oligodendrocytes in lesion sites that do not appear to form mature myelin, surmising an interruption in maturation (*49*). In a toxin-mediated model of demyelination, AMPAR activity on newly proliferated OPCs was required for remyelination (*50*). Glutamate dysregulation is not expected in the aforementioned model; however, these data support that perturbations in glutamate homeostasis as observed in the EAE model may perturb the remyelination process. Thus, approaches to regulating glutamate homeostasis may reduce demyelination and promote remyelination. Our studies used inducible deletion of the GluA4 AMPAR in the adult mouse using the PLPcreER promoter to target mature myelin. However, future studies that target AMPARs in newly proliferated OPCs in inflammatory models of demyelination would be of interest.

Axonal damage is one of the best predictors of disability in MS (*51*); therefore, preventing demyelination and/or promoting remyelination has important implications for the preservation of axonal integrity. In the present study, we observed decreased clinical symptoms in the chronic phase of EAE consistent with reduced demyelination and loss of myelinated axons in mice with targeted deletion of AMPAR function in mature oligodendrocytes. Hypomyelinated axons are more susceptible to excitotoxic damage than myelinated axons (*52*), suggesting that damage to oligodendrocytes can enhance susceptibility of axons to excitotoxicity and other insults. In addition, oligodendrocytes provide metabolic support to axons in the form of lactate, suggesting that disruption of myelin can interrupt this support mechanism (*53*). In our study, only myelinated axon numbers were affected by AMPAR deletion from mature oligodendrocytes, indicating that for myelinated axons in EAE, axonal damage may be secondary to myelin damage.

In the present study, we also observed reduced immunostaining for Iba1 in spinal cords from AMPAR-deficient mice compared to controls subjected to EAE but not GFAP (a marker of astrocytes). In our study, clinical scores were reduced in the chronic phase of the disease in AMPAR-deficient mice concomitant with improved myelinated axon integrity. Previous studies have shown that markers of the myeloid lineage correlate with disease severity and removal of myelin debris (*24*). Therefore, our observed reduction in Iba1-immunopositive staining is likely a consequence of reduced damage to myelin and axons. Alternatively, single-cell analysis of postmortem MS brains and spinal cords from mice induced with EAE shows that oligodendrocytes express many genes associated with immune responses (*54*), suggesting the possibility that preventing myelin damage may contribute to altered inflammatory responses (*55*). It is also possible that glutamate signaling in oligodendrocytes via the AMPAR could alter oligodendrocyte immune responses; for example, by altering expression of major histocompatibility complex molecules, pattern recognition receptors, chemokine receptors, or chemokines and cytokines. Disruption of any of these signaling factors could decrease oligodendrocyte-microglia cross-talk, thereby dampening microglial activation as observed in the PLPcreER^{+};GluA4$^{fl/fl}$ EAE mice. How and whether AMPAR signaling plays a role in oligodendrocyte and microglial interactions will require further investigation.

There is limited evidence that current therapies available for MS prevent disease progression (*2*), advocating for the discovery of targets that can protect the CNS during inflammatory events. Our results indicate that a reduction in AMPAR function in mature oligodendrocytes reduces not only demyelination but also axonal loss in EAE, emphasizing glutamate dysfunction as an important underlying neurodegenerative mechanism in MS. Since glutamatergic homeostasis is critical for normal physiological processes, many considerations must be made in regard to therapeutic efficacy. In addition, clinically approved drugs that target ionotropic receptors tend to be partial antagonists. Since NMDAR activation occurs downstream of AMPAR, perhaps a combination approach would be more advantageous. In addition, treatment strategies that regulate glutamate homeostasis would likely benefit as add-on therapies to currently prescribed immune modulators in MS. Overall, these data provide the first direct evidence that blocking AMPAR-mediated excitotoxicity selectively to myelin attenuates axonal demise, providing a promising therapeutic target for neurodegeneration in MS.

MATERIALS AND METHODS

Primary cultures and calcium imaging of mature oligodendrocytes

Oligodendrocytes were obtained from postnatal day (P) 2 or P3 Long-Evans rats as previously described (*8*, *56*). Purified oligodendrocytes were plated onto poly-DL-ornithine–coated glass coverslips in 12-well plates and maintained in basal-defined media [Dulbecco's minimum essential medium containing 4 mM L-glutamine, 1 mM pyruvic acid, bovine serum albumin (1 mg/ml), human apo-transferrin (50 mg/ml), bovine pancreatic insulin (5 mg/ml), 30 nM sodium selenite, 10 nM D-biotin, and 10 nM hydrocortisone] supplemented with recombinant basic fibroblast growth factor (10 ng/ml; PeproTech, RockyHill, NJ) and human platelet-derived growth factor (10 ng/ml; PeproTech) for 7 days. To promote differentiation into mature

(myelin-producing) oligodendrocytes, cells were then cultured for another 7 days in basal-defined media containing triiodothyronine (3 ng/ml; PeproTech) and ciliary neurotrophic factor (10 ng/ml; PeproTech). Primary cultured mature oligodendrocytes identified as MBP-expressing cells were used in these studies. Calcium imaging was performed as previously described (*57*). Mature oligodendrocytes on coverslips were loaded with the calcium-sensitive Fura-2 dye by exposing cells to the standard artificial CSF (aCSF; 140 mM NaCl, 5 mM KCl, 1.5 mM $CaCl_2$, 1.5 mM $MgCl_2$, 10 mM Hepes, and NaOH to pH 7.4 at 37°C) containing 5 to 10 μM of the cell-permeant Fura-2 AM and 0.01% of the dispersing agent Pluronic F-127 (Invitrogen, Molecular Probes, Grand Island, NY) for 15 to 40 min at 37°C. An individual coverslip was mounted and formed on the base of a flow-through perfusion chamber (RC-25, Warner Instruments, Hamden, CT). The chamber was then secured to the stage of an IX-70 inverted Olympus microscope with an attached high-speed wavelength changer (Lambda DG-4, Sutter Instrument, Novato, CA) and a mounted digital charge-coupled device camera (Orca II, Hamamatsu, Bridgewater, NJ). The temperature of the perfusate was maintained at ~37°C by an automatic temperature controller (TC-334B, Warner Instruments). Cells were alternately excited with 340- and 380-nm light, and the emitted fluorescence (I_{340} and I_{380}, respectively) was filtered at 510 ± 20 nm. Data are reported as I_{340}/I_{380}. Images were acquired, and data were analyzed using MetaFluor software (Universal Imaging, Westchester, PA). Fluorescence measurements from drawn regions of interest around the soma were obtained from image files.

Animals

Male and female mice on the C57BL/6J background were used for EAE experiments. B6.Cg-Tg(Plp1-cre/ERT)3Pop/J (referred to as PLPcreER; 005975, the Jackson laboratory) mice were crossed with $Gria4^{tm1Mony}$ mice (*18*) on a C57BL/6 background provided by H. Monyer at Heidelberg University (referred to as GluA4). For cre-driven expression of the red fluorescent protein tdTomato, mice were bred with B6;129S6-$Gt(ROSA)26Sor^{tm14(CAG-tdTomato)Hze}$/J mice (referred to as tdTomato; 007908, the Jackson laboratory). EAE was performed on 8- to 10-week-old PLPcreER mice. Littermate controls were used for all experiments. Animals were housed and treated in accordance with National Institutes of Health (NIH) and the Institutional Animal Care and Use Committee guidelines of the University of Alabama at Birmingham and the Cleveland Clinic.

Tamoxifen induction

PLPcreER mice and littermate controls received intraperitoneal injections of tamoxifen (20 mg/ml) (approximately 75 mg/kg; T5648, Sigma-Aldrich, St. Louis, MO) in 100 μl of peanut oil every day for 5 days, 2 to 3 weeks before induction of EAE. For calcium imaging experiments that used $PLPcreER^{+}$;$tdTomato^{+}$ mice at P9, one intraperitoneal injection of 30 μl of tamoxifen (10 mg/ml) in peanut oil was given at P3.

EAE induction and scoring

Mice were induced with EAE as previously described (*8*) using a 200-μl emulsion containing 50 μg of myelin oligodendrocyte glycoprotein 35-55 (CPC Scientific, Sunnyvale, CA) and 125 μg of desiccated *Mycobacterium tuberculosis* H37Ra (Difco Laboratories, Detroit, MI) in incomplete Freund's adjuvant (Becton, Dickinson and Company, Sparks, MD) or using a custom emulsion containing the same doses from Hooke Laboratories (Lawrence, MA). Intraperitoneal injections of 200 ng of *Bordetella pertussis* toxin (List Biological Laboratories, Campbell, CA or Hooke Laboratories, Lawrence, MA) in phosphate-buffered saline (PBS) were administered on days 0 and 2 of induction. Mice were scored daily for symptoms of EAE using the following scale: 0, no symptoms; 1, loss of tail tone; 2, flaccid tail; 3, partial hind limb paralysis; 4, complete hind limb paralysis; 5, moribund state (humanely euthanized); and 6, death.

Perfusion and preparation of mouse spinal cords for immunohistochemistry

Spinal cords from mice were removed following transcardiac perfusion with 4% paraformaldehyde (PFA) in PBS, postfixed overnight, and cryopreserved in 30% sucrose. For adult mice, spinal cords were decalcified in 0.5 M EDTA in PBS (pH 7.8) for 3 weeks before cryopreservation. Spinal cords were cut into six pieces and embedded in a solution of one part 30% sucrose in PBS/two parts Optimal Cutting Temperature (OCT) Compound embedding medium (Fisher HealthCare, Waltham, MA). Sections were cut on a cryostat at 16 μm (or 30 μm for confocal 3D reconstructions).

DAB immunohistochemistry

Antigen retrieval was performed using 10 mM citrate buffer (pH 3) at 37°C for 30 min. Sections were blocked in 5% serum corresponding to the host of the secondary antibody with 0.3% Triton X-100 in PBS for 30 min to 1 hour at room temperature. Primary antibodies were diluted in blocking buffer and incubated on sections overnight at 4°C. Biotinylated secondary antibodies were diluted in blocking buffer and incubated on sections for 1 hour at room temperature. Endogenous peroxidase activity was blocked by incubating slices in 0.3% hydrogen peroxide in methanol for 10 min at room temperature. Antibodies were visualized using the avidin-biotin-immunoperoxidase complex (ABC) method using the VECTASTAIN ABC Kit (PK-4000, Vector Laboratories, Burlingame, CA) and DAB Peroxidase (horseradish peroxidase) Substrate Kit (SK-4100, Vector Laboratories, Burlingame, CA). Slides were dehydrated and mounted in Permount (SP15, Thermo Fisher Scientific, Waltham, MA). Primary antibodies included goat polyclonal anti-MBP (D-18) immunoglobulin G (IgG) (1:1000; sc-13912, Santa Cruz Biotechnology, Dallas, TX), mouse anti-GFAP IgG2b (1:1000; 835301, BioLegend, San Diego, CA), rabbit anti-Iba1 (1:750; 019-19741, Wako, Richmond, VA), and rabbit anti-APP A4 [Y188] IgG (1:750; ab32136, Abcam, Cambridge, UK). Biotinylated secondary antibodies were used at a dilution of 1:200 and included horse anti-mouse IgG (BA-2000, Vector Laboratories, Burlingame, CA), goat anti-rabbit IgG (BA-1000, Vector Laboratories, Burlingame, CA), and horse anti-goat IgG (BA-9500, Vector Laboratories, Burlingame, CA).

Immunofluorescence

Antigen retrieval was performed on anti-GluA3 and anti-Iba1 immunofluorescence sections using 10 mM citrate buffer (pH 3) at 37°C for 30 min. Sections were blocked in 5% serum corresponding to the host of the secondary antibody with 0.3% Triton X-100 in PBS (PBS alone for anti-GluA3) for 1 hour at room temperature. Primary antibodies were diluted in blocking buffer and incubated on sections overnight at 4°C or for 4 hours at room temperature.

Secondary antibodies (biotinylated for anti–GluA1-3 and antibodies stained with DyLight 405; fluorescence conjugated for all others) were diluted in blocking buffer and incubated on sections for 1 hour at room temperature. For tissue treated with biotinylated

secondary antibodies, fluorescence-conjugated streptavidin was diluted in washing buffer and incubated on sections for 30 min at room temperature. Slides were mounted with Fluoromount-G (0100-01, SouthernBiotech, Birmingham, AL) containing bisbenzimide (1:1000; H3569, Invitrogen, Carlsbad, CA) where applicable.

Primary antibodies included mouse anti-CC1 (1:200; OP80, Calbiochem/MilliporeSigma, Burlington, MA), goat polyclonal anti-MBP (D-18) IgG (1:250; sc-13912, Santa Cruz Biotechnology, Dallas, TX), mouse anti-NeuN IgG1 (1:750; MAB377, EMD Millipore, Billerica, MA), mouse anti-GFAP IgG2b (1:1000 or 1:600 with DyLight 405; 835301, BioLegend, San Diego, CA), rabbit anti-Iba1 (1:750 or 1:500 with DyLight 405; 019-19741, Wako, Richmond, VA), goat anti-Iba1 (1:200; ab107159, Abcam, Cambridge, UK), rabbit anti-GluA1 (1:500; AB1504, EMD Millipore, Billerica, MA), mouse anti-GluA2 IgG2a (1:100; MAB397, EMD Millipore, Billerica, MA), rabbit anti-GluA2 (1:200; AB1768-I, EMD Millipore, Billerica, MA), rabbit anti-GluA3 (1:25; 4676S, Cell Signaling Technology, Danvers, MA), rabbit anti-GluA4 (1:300; AB1508, EMD Millipore, Billerica, MA), rabbit anti-APP A4 (Y188) IgG (1:500; ab32136, Abcam, Cambridge, UK), and mouse anti-neurofilament marker (SMI-312) IgG1/IgM (1:2000; 837901, BioLegend, San Diego, CA).

Biotinylated secondary antibodies were used at 1:200 and included horse anti-mouse IgG (BA-2000, Vector Laboratories, Burlingame, CA) and goat anti-rabbit IgG (BA-1000, Vector Laboratories, Burlingame, CA). Fluorescence-conjugated secondary antibodies were used at 1:1000 or 1:500 (all from Invitrogen, Carlsbad, CA) and included Alexa Fluor 488 goat anti-mouse IgG (A11001), Alexa Fluor 488 goat anti-rabbit IgG (A11034), Alexa Fluor 488 donkey anti-goat IgG (A11055), Alexa Fluor 488 goat anti-mouse IgG/IgM (A10680), Alexa Fluor 594 goat anti-rabbit IgG (A11037), Alexa Fluor 647 goat anti-mouse IgG (A21235), Alexa Fluor 647 goat anti-rabbit IgG (A21245), and Alexa Fluor 647 donkey anti-rabbit IgG (A31573). Fluorescence-conjugated streptavidins (all from Invitrogen) included streptavidin protein DyLight 488 (1:1000; 212832), Alexa Fluor 647–conjugated streptavidin (1:1000; lyophilized stock diluted 1 mg/ml in PBS; S21374), and streptavidin protein DyLight 405 (1:500; 21831).

Imaging

DAB immunohistochemical images were acquired using a Leica DM5500 B upright microscope with 5× objective and Leica DFC425 C digital camera with Leica Application Suite (version 4.4.0) acquisition software or a Leica SCN400 slide scanner at ×40 magnification. Toluidine blue staining images were acquired using a Leica SCN400 slide scanner at ×40 magnification. Fluorescent confocal images were acquired using a Nikon C2 confocal microscope system (Nikon, Melville, NY) with NIS-Elements software (Nikon, Melville, NY). Confocal images for 3D reconstruction were captured with 0.3-μm step size using the following objectives: Plan Fluor 40×/1.30 numerical aperture (NA) (oil immersion) and Apo 60×/1.40 NA (oil immersion). An advanced noise removal algorithm was applied evenly across experimental groups. For electron microscopy, grids were examined on a Tecnai G2 SpiritBT transmission electron microscope (FEI Company, Hillsboro, OR) operated at 60 kV.

Quantification of glutamate receptor subunits by immunohistochemistry

Percent area staining of AMPAR subunits GluA1-4 was calculated for cells containing bisbenzimide in four fields per animal taken from four sections including every fifth serial 16-μm section. Confocal images were taken at ×40 magnification with 170 μm by 170 μm fields for CC1, GFAP, and Iba1 and 200 μm by 200 μm fields for NeuN. Manual thresholding was performed using NIS-Elements software (Nikon, Melville, NY) in a blinded manner after background subtraction to identify staining for GFAP- and Iba1-immunopositive processes, for CC1- or NeuN-immunopositive cells containing bisbenzimide, and to detect area of GluA1-4 staining. For quantification of GluA4 in $CC1^-$ cells, bisbenzimide in the absence of CC1 immunoreactivity was used to identify $CC1^-$ cells, and GluA4 surrounding bisbenzimide was considered $GluA4^+CC1^-$. Cells were counted in a blinded manner using NIH ImageJ software, 1.48v.

Quantitative real-time reverse transcription polymerase chain reaction analysis

Optic nerves were removed from mice after transcardiac perfusion with cold, sterile PBS, and RNA was extracted using the RNeasy Mini Kit (74104, QIAGEN, Hilden, Germany) according to the manufacturer's protocol. RNA concentration was measured using a NanoDrop One (Thermo Fisher Scientific, Waltham, MA), and any remaining DNA contamination was removed by treatment with deoxyribonuclease I (18068015, Invitrogen, Carlsbad, CA). The complementary DNA was synthesized using TaqMan Reverse Transcription Reagents (N8080234, Invitrogen, Carlsbad, CA). Quantitative real-time reverse transcription polymerase chain reactions (PCR) were made using TaqMan Fast Advanced Master Mix (4444556, Applied Biosystems, Foster City, CA) and predeveloped TaqMan gene expression probes. Reactions were analyzed on a QuantStudio 6 Flex Real-Time PCR System using QuantStudio 6 software (Applied Biosystems, Foster City, CA). Samples were run in triplicate for each gene, and data were averaged for analysis. Fold change was calculated as $2^{-\Delta\Delta Ct}$ compared to $PLPcreER^+;GluA4^{fl/fl}$ (WT) values. Gene expression levels were normalized to glyceraldehyde-3-phosphate dehydrogenase.

Quantification of reactive gliosis

Percent area stained with Iba1 and GFAP antibodies were analyzed in thoracic and lumbar spinal cord sections using the free NIH ImageJ software, 1.48v, as previously described (*8*, *58*). Briefly, images were converted to 16 bit, and whole spinal cords were traced. The rolling ball with sliding paraboloid method set to a radius of 4.0 pixels for Iba1 and 50.0 pixels for GFAP was used for background subtraction. Threshold was set to the same baseline across experimental groups to measure area of cellular staining. Assessments were made on every fifth section from 16-μm serial sections from the lumbar and thoracic regions of the spinal cord.

Quantification of MBP staining

OD of MBP staining was analyzed in thoracic and lumbar spinal cord sections using the free NIH ImageJ software, 1.48v, as previously described (*58*). Briefly, white matter regions of the spinal cord were traced, and mean gray values were obtained from every fifth section from 16-μm serial sections from the lumbar and thoracic regions of the spinal cord. These values were converted into OD values using the following formula, as described in the ImageJ User Guide IJ 1.46r: $OD = \log_{10}(255/\text{mean gray value})$.

Quantification of APP-immunopositive puncta

Numbers of APP^+ puncta were counted in lumbar spinal cords of PLPcreER;GluA4 mice using the free NIH ImageJ software, 1.48v.

Images were converted to grayscale and dorsal white matter columns were traced. Background was subtracted from images using the rolling ball with sliding paraboloid method set to a radius of 35.0 pixels. Threshold was set to the same baseline across experimental groups to measure particles more than 4 μm^2. Assessments were made every fifth section on 16-μm serial sections.

Quantification of SMI-312–immunopositive axons

Numbers of SMI-312$^+$ axons in the ventral white matter of PLPcreER$^+$;GluA4$^{fl/fl}$ and PLPcreER$^-$;GluA4$^{fl/fl}$ mouse spinal cords were measured from 3D reconstructions of immunofluorescence staining. Confocal 3D 133 μm by 133 μm by 25.50 μm *z*-stacks were subjected to blinded manual thresholding, and numbers of axons were automatically counted with NIS-Elements software (Nikon, Melville, NY). Objects with a volume of less than 0.015 μm^3 and a sphericity of less than 0.350 were removed from analyses, as these objects were determined to be nonaxonal. Assessments were made on every fifth serial 30-μm section, with four fields from two sections (including right and left ventral white matter).

Toluidine blue staining and electron microscopy preparation

Mice were perfused with 4% PFA, 2% glutaraldehyde in 0.1 M sodium cacodylate buffer at pH 7.4. Spinal cords were removed, and lumbar regions were processed by the Cleveland Clinic Electron Microscopy Core. Tissue was postfixed in 1% osmium tetroxide in water, stained with 1% uranyl acetate in maleate buffer (pH 5.1), and dehydrated with ethanol and propylene oxide before being embedded in Pure Eponate 12 resin (Ted Pella Inc., Redding, CA). Semithin 1-μm sections were cut with a diamond knife and stained with toluidine blue for analysis by light microscopy. Ultrathin 85-nm sections were cut with a diamond knife, stained with uranyl acetate and lead citrate, and observed with a transmission electron microscope.

Analysis of toluidine blue

Six 74.53 μm by 60.43 μm fields across the ventral funiculus of the spinal cord were analyzed per mouse. All myelinated axons in each field were counted and calculated as number of axons per square millimeter.

Analysis of electron microscopy

Six 20.75 μm by 13.68 μm images taken at ×6800 magnification were used to measure g-ratios in naïve mice. All myelinated axons in each image were traced in ImageJ 1.52i, and g-ratios were calculated as axon diameter divided by axon and myelin diameter. Six 49.35 μm by 32.54 μm images taken at ×2900 magnification were used to count axons in naïve and EAE mice across the ventral funiculus of the spinal cord. All axons in each image were counted and calculated as number of axons per square millimeters.

Calcium imaging in ex vivo optic nerves

Calcium imaging was performed on the basis of previously described protocols (*59*, *60*). PLPcreER$^+$;GluA4$^{fl/fl}$;tdTomato$^+$ and PLPcreER$^+$;GluA4$^{+/+}$;tdTomato$^+$ mice were tamoxifen-induced at P3. P9 mice were anesthetized with isoflurane and decapitated, and optic nerves were removed and placed in aCSF [containing 126 mM NaCl, 26 mM $NaHCO_3$, 3.0 mM KCl, 1.25 mM NaH_2PO_4, 2.0 mM Mg_2SO_4, 2.0 mM $CaCl_2$, and 10 mM dextrose (pH 7.4)], bubbled with carbogen (5% CO_2/95% O_2) for 20 min, and retested for pH. Nerves were then incubated for 2 hours in aCSF with 40 μM OGB-1 AM (O6807, Invitrogen, Carlsbad, CA) at room temperature with constant carbogen bubbling. Optic nerves were washed in aCSF and mounted in a perfusion chamber with a glass bottom made of a #1 coverslip. The chamber was perfused with room-temperature carbogenated aCSF and 10 μM cyclothiazide (CTZ; 0713, Tocris Bioscience, Bristol, UK) and mounted on a Nikon Eclipse Ti-S inverted microscope (Nikon, Melville, NY), with Nikon C2 confocal microscope system (Nikon, Melville, NY). Glutamate (100 μM; G1626, Sigma-Aldrich, St. Louis, MO) and NBQX (100 μM; 1044, Tocris Bioscience) were used for stimulation with CTZ (10 μM). Between stimulation with glutamate + CTZ and NBQX + glutamate + CTZ, optic nerves were given a 10-min recovery period in aCSF + CTZ. Time-lapse images were taken at 4.3- to 10-s intervals using a Plan Fluor 40×/1.30 NA (oil immersion) objective. OGB-1 was excited at 488 nm. Intensity of green fluorescence was normalized as $\Delta F/F_0$ ($\Delta F/F_0 = [(F - F_B) - (F_0 - F_B)]/(F_0 - F_B)$), where F was raw fluorescence signal, F_B was background, and F_0 was mean fluorescence signal in a baseline period that included the first 30 s before stimulus. Absolute calcium levels were not reported. Data were analyzed using NIS-Elements software (Nikon, Melville, NY) and Microsoft Excel. For analysis, only tdTomato$^+$ oligodendrocyte cell bodies were traced and fluorescence intensity was measured.

Statistical analysis

All statistical analyses were performed using GraphPad Prism software version 5.03 or 8.0.2 (GraphPad Software, La Jolla, CA). Specific analyses performed including P values are reported where indicated.

SUPPLEMENTARY MATERIALS

Supplementary material for this article is available at http://advances.sciencemag.org/cgi/content/full/6/2/eaax5936/DC1

Fig. S1. AMPARs mediate most of the intracellular Ca_i^{2+} responses in primary cultured mature oligodendrocyte somas.

Fig. S2. GluA4 expression is selectively reduced in CC1$^+$ cells from PLPcreER$^+$;GluA4$^{fl/fl}$ compared to PLPcreER$^-$;GluA4$^{fl/fl}$ mice.

Fig. S3. AMPAR subunits GluA1-3 are not changed in adult spinal cord oligodendrocytes from PLPcreER$^+$;GluA4$^{fl/fl}$ compared to PLPcreER$^-$;GluA4$^{fl/fl}$ mice.

Fig. S4. GluA4 transcript expression is reduced in PLPcreER$^+$;GluA4$^{fl/fl}$ mouse white matter.

Fig. S5. Myelin is unaltered in naïve PLPCreER$^+$:GluA4$^{fl/fl}$ mice.

Fig. S6. Frequencies of myelin g-ratio and axon diameter are unchanged in naïve PLPCreER$^+$:GluA4$^{fl/fl}$ mice.

Fig. S7. TdTomato expression is predominately limited to oligodendrocytes in EAE PLPcreER$^+$;tdTomato$^+$ mice.

Fig. S8. The GluA4 AMPAR subunit remains reduced in oligodendrocytes from PLPcreER$^+$;GluA4$^{fl/fl}$ mice subjected to EAE.

Movie S1. 3D representation of myelin and axons from a PLPcreER$^-$;GluA4$^{fl/fl}$ (WT) mouse.

Movie S2. 3D representation of myelin and axons from a PLPcreER$^+$;GluA4$^{fl/fl}$ (KO) mouse.

View/request a protocol for this paper from *Bio-protocol*.

REFERENCES AND NOTES

1. E. W. Willoughby, E. Grochowski, D. K. B. Li, J. Oger, L. F. Kastrukoff, D. W. Paty, Serial magnetic resonance scanning in multiple sclerosis: A second prospective study in relapsing patients. *Ann. Neurol.* **25**, 43–49 (1989).
2. B. Smith, S. Carson, R. Fu, M. McDonagh, T. Dana, B. K. S. Chan, S. Thakurta, A. Gibler, in *Drug Class Review: Disease-modifying Drugs for Multiple Sclerosis: Final Update 1 Report* (Oregon Health & Science University, 2010).
3. J. F. Stover, U. E. Pleines, M. C. Morganti-Kossmann, T. Kossmann, K. Lowitzsch, O. S. Kempski, Neurotransmitters in cerebrospinal fluid reflect pathological activity. *Eur. J. Clin. Invest.* **27**, 1038–1043 (1997).
4. O. Pampliega, M. Domercq, P. Villoslada, J. Sepulcre, A. Rodríguez-Antigüedad, C. Matute, Association of an EAAT2 polymorphism with higher glutamate concentration in relapsing multiple sclerosis. *J. Neuroimmunol.* **195**, 194–198 (2008).

5. R. Srinivasan, N. Sailasuta, R. Hurd, S. Nelson, D. Pelletier, Evidence of elevated glutamate in multiple sclerosis using magnetic resonance spectroscopy at 3 T. *Brain* **128**, 1016–1025 (2005).
6. C. J. Azevedo, J. Kornak, P. Chu, M. Sampat, D. T. Okuda, B. A. Cree, S. J. Nelson, S. L. Hauser, D. Pelletier, In vivo evidence of glutamate toxicity in multiple sclerosis. *Ann. Neurol.* **76**, 269–278 (2014).
7. A. M. Klauser, O. T. Wiebenga, A. J. C. Eijlers, M. M. Schoonheim, B. M. J. Uitdehaag, F. Barkhof, P. J. W. Pouwels, J. J. G. Geurts, Metabolites predict lesion formation and severity in relapsing-remitting multiple sclerosis. *Mult. Scler.* **24**, 491–500 (2018).
8. K. S. Evonuk, B. J. Baker, R. E. Doyle, C. E. Moseley, C. M. Sestero, B. P. Johnston, P. de Sarno, A. Tang, I. Gembitsky, S. J. Hewett, C. T. Weaver, C. Raman, T. M. DeSilva, Inhibition of system$_{xc}^-$ transporter attenuates autoimmune inflammatory demyelination. *J. Immunol.* **195**, 450–463 (2015).
9. D. Pitt, P. Werner, C. S. Raine, Glutamate excitotoxicity in a model of multiple sclerosis. *Nat. Med.* **6**, 67–70 (2000).
10. T. Smith, A. Groom, B. Zhu, L. Turski, Autoimmune encephalomyelitis ameliorated by AMPA antagonists. *Nat. Med.* **6**, 62–66 (2000).
11. P. Bannerman, M. Horiuchi, D. Feldman, A. Hahn, A. Itoh, J. See, Z. P. Jia, T. Itoh, D. Pleasure, GluR2-free α-amino-3-hydroxy-5-methyl-4-isoxazolepropionate receptors intensify demyelination in experimental autoimmune encephalomyelitis. *J. Neurochem.* **102**, 1064–1070 (2007).
12. A. A. Boldyrev, V. I. Kazey, T. A. Leinsoo, A. P. Mashkina, O. V. Tyulina, P. Johnson, J. O. Tuneva, S. Chittur, D. O. Carpenter, Rodent lymphocytes express functionally active glutamate receptors. *Biochem. Biophys. Res. Commun.* **324**, 133–139 (2004).
13. Y. Ganor, M. Besser, N. Ben-Zakay, T. Unger, M. Levite, Human T cells express a functional ionotropic glutamate receptor GluR3, and glutamate by itself triggers integrin-mediated adhesion to laminin and fibronectin and chemotactic migration. *J. Immunol.* **170**, 4362–4372 (2003).
14. T. M. DeSilva, P. A. Rosenberg, in *Biology of the Oligodendrocyte* (Cambridge Press, 2012), chap. 10.
15. P. C. Christensen, Z. Samadi-Bahrami, V. Pavlov, P. K. Stys, G. R. W. Moore, Ionotropic glutamate receptor expression in human white matter. *Neurosci. Lett.* **630**, 1–8 (2016).
16. F. Guo, Y. Maeda, E. M. Ko, M. Delgado, M. Horiuchi, A. Soulika, L. Miers, T. Burns, T. Itoh, H. Shen, E. Lee, J. Sohn, D. Pleasure, Disruption of NMDA receptors in oligodendroglial lineage cells does not alter their susceptibility to experimental autoimmune encephalomyelitis or their normal development. *J. Neurosci.* **32**, 639–645 (2012).
17. N. H. Doerflinger, W. B. Macklin, B. Popko, Inducible site-specific recombination in myelinating cells. *Genesis* **35**, 63–72 (2003).
18. E. C. Fuchs, A. R. Zivkovic, M. O. Cunningham, S. Middleton, F. E. N. LeBeau, D. M. Bannerman, A. Rozov, M. A. Whittington, R. D. Traub, J. N. P. Rawlins, H. Monyer, Recruitment of parvalbumin-positive interneurons determines hippocampal function and associated behavior. *Neuron* **53**, 591–604 (2007).
19. D. M. Talos, R. E. Fishman, H. Park, R. D. Folkerth, P. L. Follett, J. J. Volpe, F. E. Jensen, Developmental regulation of α-amino-3-hydroxy-5-methyl-4-isoxazole-propionic acid receptor subunit expression in forebrain and relationship to regional susceptibility to hypoxic/ischemic injury. I. Rodent cerebral white matter and cortex. *J. Comp. Neurol.* **497**, 42–60 (2006).
20. D. M. Talos, P. L. Follett, R. D. Folkerth, R. E. Fishman, F. L. Trachtenberg, J. J. Volpe, F. E. Jensen, Developmental regulation of α-amino-3-hydroxy-5-methyl-4-isoxazole-propionic acid receptor subunit expression in forebrain and relationship to regional susceptibility to hypoxic/ischemic injury. II. Human cerebral white matter and cortex. *J. Comp. Neurol.* **497**, 61–77 (2006).
21. S. Li, P. K. Stys, Mechanisms of ionotropic glutamate receptor-mediated excitotoxicity in isolated spinal cord white matter. *J. Neurosci.* **20**, 1190–1198 (2000).
22. C. Matute, M. V. Sánchez-Gómez, L. Martínez-Millán, R. Miledi, Glutamate receptor-mediated toxicity in optic nerve oligodendrocytes. *Proc. Natl. Acad. Sci. U.S.A.* **94**, 8830–8835 (1997).
23. E. Kougioumtzidou, T. Shimizu, N. B. Hamilton, K. Tohyama, R. Sprengel, H. Monyer, D. Attwell, W. D. Richardson, Signalling through AMPA receptors on oligodendrocyte precursors promotes myelination by enhancing oligodendrocyte survival. *eLife* **6**, e28080 (2017).
24. R. Yamasaki, H. Lu, O. Butovsky, N. Ohno, A. M. Rietsch, R. Cialic, P. M. Wu, C. E. Doykan, J. Lin, A. C. Cotleur, G. Kidd, M. M. Zorlu, N. Sun, W. Hu, L. P. Liu, J.-C. Lee, S. E. Taylor, L. Uehlein, D. Dixon, J. Gu, C. M. Floruta, M. Zhu, I. F. Charo, H. L. Weiner, R. M. Ransohoff, Differential roles of microglia and monocytes in the inflamed central nervous system. *J. Exp. Med.* **211**, 1533–1549 (2014).
25. B. D. Trapp, J. Peterson, R. M. Ransohoff, R. Rudick, S. Mörk, L. Bö, Axonal transection in the lesions of multiple sclerosis. *N. Engl. J. Med.* **338**, 278–285 (1998).
26. B. Ferguson, M. K. Matyszak, M. M. Esiri, V. H. Perry, Axonal damage in acute multiple sclerosis lesions. *Brain* **120** (Pt. 3), 393–399 (1997).
27. T. Kuhlmann, G. Lingfeld, A. Bitsch, J. Schuchardt, W. Bruck, Acute axonal damage in multiple sclerosis is most extensive in early disease stages and decreases over time. *Brain* **125**, 2202–2212 (2002).
28. P. L. Follett, P. A. Rosenberg, J. J. Volpe, F. E. Jensen, NBQX attenuates excitotoxic injury in developing white matter. *J. Neurosci.* **20**, 9235–9241 (2000).
29. S. M. Manning, D. M. Talos, C. Zhou, D. B. Selip, H.-K. Park, C.-J. Park, J. J. Volpe, F. E. Jensen, NMDA receptor blockade with memantine attenuates white matter injury in a rat model of periventricular leukomalacia. *J. Neurosci.* **28**, 6670–6678 (2008).
30. I. Micu, Q. Jiang, E. Coderre, A. Ridsdale, L. Zhang, J. Woulfe, X. Yin, B. D. Trapp, J. E. McRory, R. Rehak, G. W. Zamponi, W. Wang, P. K. Stys, NMDA receptors mediate calcium accumulation in myelin during chemical ischaemia. *Nature* **439**, 988–992 (2006).
31. J. W. McDonald, S. P. Althomsons, K. L. Hyrc, D. W. Choi, M. P. Goldberg, Oligodendrocytes from forebrain are highly vulnerable to AMPA/kainate receptor-mediated excitotoxicity. *Nat. Med.* **4**, 291–297 (1998).
32. R. Káradóttir, P. Cavelier, L. H. Bergersen, D. Attwell, NMDA receptors are expressed in oligodendrocytes and activated in ischaemia. *Nature* **438**, 1162–1166 (2005).
33. J. C. Piña-Crespo, M. Talantova, I. Micu, B. States, H.-S. V. Chen, S. Tu, N. Nakanishi, G. Tong, D. Zhang, S. F. Heinemann, G. W. Zamponi, P. K. Stys, S. A. Lipton, Excitatory glycine responses of CNS myelin mediated by NR1/NR3 "NMDA" receptor subunits. *J. Neurosci.* **30**, 11501–11505 (2010).
34. R. J. Bridges, N. R. Natale, S. A. Patel, System x_c^- cystine/glutamate antiporter: An update on molecular pharmacology and roles within the CNS. *Br. J. Pharmacol.* **165**, 20–34 (2012).
35. O. Pampliega, M. Domercq, F. N. Soria, P. Villoslada, A. Rodríguez-Antigüedad, C. Matute, Increased expression of cystine/glutamate antiporter in multiple sclerosis. *J. Neuroinflammation* **8**, 63 (2011).
36. K. Tanaka, K. Watase, T. Manabe, K. Yamada, M. Watanabe, K. Takahashi, H. Iwama, T. Nishikawa, N. Ichihara, T. Kikuchi, S. Okuyama, N. Kawashima, S. Hori, M. Takimoto, K. Wada, Epilepsy and exacerbation of brain injury in mice lacking the glutamate transporter GLT-1. *Science* **276**, 1699–1702 (1997).
37. M. K. Sharief, R. Hentges, Association between tumor necrosis factor-α and disease progression in patients with multiple sclerosis. *N. Engl. J. Med.* **325**, 467–472 (1991).
38. A. E. Juedes, P. Hjelmstrom, C. M. Bergman, A. L. Neild, N. H. Ruddle, Kinetics and cellular origin of cytokines in the central nervous system: Insight into mechanisms of myelin oligodendrocyte glycoprotein-induced experimental autoimmune encephalomyelitis. *J. Immunol.* **164**, 419–426 (2000).
39. T. Korn, T. Magnus, S. Jung, Autoantigen specific T cells inhibit glutamate uptake in astrocytes by decreasing expression of astrocytic glutamate transporter GLAST: A mechanism mediated by tumor necrosis factor-α. *FASEB J.* **19**, 1878–1880 (2005).
40. S. Hu, W. S. Sheng, L. C. Ehrlich, P. K. Peterson, C. C. Chao, Cytokine effects on glutamate uptake by human astrocytes. *Neuroimmunomodulation* **7**, 153–159 (2000).
41. M. Ohgoh, T. Hanada, T. Smith, T. Hashimoto, M. Ueno, Y. Yamanishi, M. Watanabe, Y. Nishizawa, Altered expression of glutamate transporters in experimental autoimmune encephalomyelitis. *J. Neuroimmunol.* **125**, 170–178 (2002).
42. K. Mitosek-Szewczyk, G. Sulkowski, Z. Stelmasiak, L. Struzynska, Expression of glutamate transporters GLT-1 and GLAST in different regions of rat brain during the course of experimental autoimmune encephalomyelitis. *Neuroscience* **155**, 45–52 (2008).
43. D. Pitt, I. E. Nagelmeier, H. C. Wilson, C. S. Raine, Glutamate uptake by oligodendrocytes: Implications for excitotoxicity in multiple sclerosis. *Neurology* **61**, 1113–1120 (2003).
44. B. A. Miller, F. Sun, R. N. Christensen, A. R. Ferguson, J. C. Bresnahan, M. S. Beattie, A sublethal dose of TNFα potentiates kainate-induced excitotoxicity in optic nerve oligodendrocytes. *Neurochem. Res.* **30**, 867–875 (2005).
45. D. Stellwagen, E. C. Beattie, J. Y. Seo, R. C. Malenka, Differential regulation of AMPA receptor and GABA receptor trafficking by tumor necrosis factor-α. *J. Neurosci.* **25**, 3219–3228 (2005).
46. J. Newcombe, A. Uddin, R. Dove, B. Patel, L. Turski, Y. Nishizawa, T. Smith, Glutamate receptor expression in multiple sclerosis lesions. *Brain Pathol.* **18**, 52–61 (2008).
47. C. F. Lucchinetti, B. F. G. Popescu, R. F. Bunyan, N. M. Moll, S. F. Roemer, H. Lassmann, W. Brück, J. E. Parisi, B. W. Scheithauer, C. Giannini, S. D. Weigand, J. Mandrekar, R. M. Ransohoff, Inflammatory cortical demyelination in early multiple sclerosis. *N. Engl. J. Med.* **365**, 2188–2197 (2011).
48. A. Boyd, H. Zhang, A. Williams, Insufficient OPC migration into demyelinated lesions is a cause of poor remyelination in MS and mouse models. *Acta Neuropathol.* **125**, 841–859 (2013).
49. A. Chang, W. W. Tourtellotte, R. Rudick, B. D. Trapp, Premyelinating oligodendrocytes in chronic lesions of multiple sclerosis. *N. Eng. J. Med.* **346**, 165–173 (2002).
50. H. O. Gautier, K. A. Evans, K. Volbracht, R. James, S. Sitnikov, I. Lundgaard, F. James, C. Lao-Peregrin, R. Reynolds, R. J. Franklin, R. T. Káradóttir, Neuronal activity regulates remyelination via glutamate signalling to oligodendrocyte progenitors. *Nat. Commun.* **6**, 8518 (2015).
51. C. Bjartmar, G. Kidd, S. Mork, R. Rudick, B. D. Trapp, Neurological disability correlates with spinal cord axonal loss and reduced *N*-acetyl aspartate in chronic multiple sclerosis patients. *Ann. Neurol.* **48**, 893–901 (2000).
52. D. Pitt, E. Gonzales, A. H. Cross, M. P. Goldberg, Dysmyelinated axons in shiverer mice are highly vulnerable to α-amino-3-hydroxy-5-methylisoxazole-4-propionic acid (AMPA) receptor-mediated toxicity. *Brain Res.* **1309**, 146–154 (2010).

53. Y. Lee, B. M. Morrison, Y. Li, S. Lengacher, M. H. Farah, P. N. Hoffman, Y. Liu, A. Tsingalia, L. Jin, P.-W. Zhang, L. Pellerin, P. J. Magistretti, J. D. Rothstein, Oligodendroglia metabolically support axons and contribute to neurodegeneration. *Nature* **487**, 443–448 (2012).
54. A. M. Falcao, D. van Bruggen, S. Marques, M. Meijer, S. Jäkel, E. Agirre, Samudyata, E. M. Floriddia, D. P. Vanichkina, C. Ffrench-Constant, A. Williams, A. O. Guerreiro-Cacais, G. Castelo-Branco, Disease-specific oligodendrocyte lineage cells arise in multiple sclerosis. *Nat. Med.* **24**, 1837–1844 (2018).
55. L. Peferoen, M. Kipp, P. van der Valk, J. M. van Noort, S. Amor, Oligodendrocyte-microglia cross-talk in the central nervous system. *Immunology* **141**, 302–313 (2014).
56. T. M. DeSilva, A. Y. Kabakov, P. E. Goldhoff, J. J. Volpe, P. A. Rosenberg, Regulation of glutamate transport in developing rat oligodendrocytes. *J. Neurosci.* **29**, 7898–7908 (2009).
57. C. M. McNicholas-Bevensee, K. B. DeAndrade, W. E. Bradley, L. J. Dell'Italia, P. A. Lucchesi, M. O. Bevensee, Activation of gadolinium-sensitive ion channels in cardiomyocytes in early adaptive stages of volume overload-induced heart failure. *Cardiovasc. Res.* **72**, 262–270 (2006).
58. K. S. Evonuk, C. E. Moseley, R. E. Doyle, C. T. Weaver, T. M. DeSilva, Determining immune system suppression versus CNS protection for pharmacological interventions in autoimmune demyelination. *J. Vis. Exp.* **2016**, e54348 (2016).
59. Y. Ren, A. Ridsdale, E. Coderre, P. K. Stys, Calcium imaging in live rat optic nerve myelinated axons in vitro using confocal laser microscopy. *J. Neurosci. Methods* **102**, 165–176 (2000).
60. N. Hamilton, P. S. Hubbard, A. M. Butt, Effects of glutamate receptor activation on NG2-glia in the rat optic nerve. *J. Anat.* **214**, 208–218 (2009).

Acknowledgments: We would like to thank J. Drazba, Director of the Cleveland Clinic Imaging Core for assistance. **Funding:** This study was supported by National Multiple Sclerosis Society, RG 4587-A-1; NSF, 1648822; National Eye Institute, RO1EY025687 and T32 EY024236-02; National Institute of Allergy and Infectious Diseases, T32 AI007051-39; National Institute of Neurological Disorders and Stroke, P30-NS069324; National Multiple Sclerosis Society Postdoctoral Fellowship, FG-1807-31882; and the Mike L. Jezdimir Transverse Myelitis Foundation. **Author contributions:** K.S.E. and T.M.D. conceived the study and designed the experiments. I.M.T. performed and analyzed the in vitro calcium imaging experiments under the supervision of M.O.B. K.S.E. performed and analyzed calcium imaging experiments in ex vivo optic nerves. C.E.M., C.T.W., and B.M. contributed to the design and interpretation of the EAE experiments. K.S.E. and R.E.D. performed and analyzed EAE experiments. K.A. and A.M.B. contributed to immunocytochemistry. K.S.E. and T.M.D. drafted the manuscript. M.O.B., B.M., and I.M.T. were involved in editing and discussion. **Competing interests:** The authors declare that they have no competing interests. **Data and materials availability:** All data needed to evaluate the conclusions in the paper are present in the paper and/or the Supplementary Materials. The GluA4$^{fl/fl}$ mouse line can be provided by H. Monyer at the University of Heidelberg pending scientific review and a completed material transfer agreement. Requests for the GluA4$^{fl/fl}$ mouse line should be submitted to H. Monyer at the University of Heidelberg. Additional data related to this paper may be requested from the authors.

Submitted 5 April 2019
Accepted 8 November 2019
Published 8 January 2020
10.1126/sciadv.aax5936

Citation: K. S. Evonuk, R. E. Doyle, C. E. Moseley, I. M. Thornell, K. Adler, A. M. Bingaman, M. O. Bevensee, C. T. Weaver, B. Min, T. M. DeSilva, Reduction of AMPA receptor activity on mature oligodendrocytes attenuates loss of myelinated axons in autoimmune neuroinflammation. *Sci. Adv.* **6**, eaax5936 (2020).